Conformational Coupling of Mg^{2+} and Ca^{2+} on the Three-State Folding of Calexcitin B†

Zoltan Gombos,‡ Isabelle Durussel,§ Mitsuhiko Ikura,‡ David R. Rose,‡ Jos A. Cox,§ and Avijit Chakrabartty*,‡

Division of Molecular and Structural Biology, Ontario Cancer Institute, and Department of Medical Biophysics, University of Toronto, Toronto, Ontario M5G 2M9, Canada, and Department of Biochemistry, University of Geneva, Geneva, CH-1211 Geneva 4, Switzerland

Received January 13, 2003; Revised Manuscript Received March 4, 2003

ABSTRACT: Calexcitin (CE) is a calcium sensor protein that has been implicated in associative learning through the Ca^{2+}-dependent inhibition of K^+ channels and activation of ryanodine receptors. CE_B, the major CE variant, was identified as a member of the sarcoplasmic Ca^{2+} binding protein family: proteins that can bind both Ca^{2+} and Mg^{2+}. We have now determined the intrinsic Ca^{2+} and Mg^{2+} binding affinities of CE_B and investigated their interplay on the folding and structure of CE_B. We find that urea denaturation of CE_B displays a three-state unfolding transition consistent with the presence of two structural domains. Through a combination of spectroscopic and denaturation studies we find that one domain likely possesses molten globule structure and contains a mixed Ca^{2+}/Mg^{2+} binding site and a Ca^{2+} binding site with weak Mg^{2+} antagonism. Furthermore, ion binding to the putative molten globule domain induces native structure formation. The other domain contains a single Ca^{2+}-specific binding site and has native structure, even in the absence of ion binding. Ca^{2+} binding to CE_B induces the formation of a recessed hydrophobic pocket. On the basis of measured ion binding affinities and intracellular ion concentrations, it appears that Mg^{2+}-CE_B represents the resting state and Ca^{2+}-CE_B corresponds to the active state, under physiological conditions.

Calcium ions (Ca^{2+}) are involved in ubiquitous signaling pathways that control processes ranging from cell growth to cell death. These pathways are triggered by increases in the levels of free Ca^{2+} followed by the ions binding to Ca^{2+} binding proteins (CaBPs)[1] and affecting downstream targets. Many CaBPs share a common Ca^{2+} binding motif, called "EF-hand" (*1*). Calexcitin (CE) belongs to the EF-hand superfamily and sarcoplasmic Ca^{2+} binding protein (SCP) family (*2*) and shows the highest sequence homology (28%) with SCP from the protochordate *Branchiostoma lanceolatum*, commonly called amphioxus.

CE has been identified in the squid optic lobe and implicated to play a role in associative learning (ASL). The involvement of CE in ASL has been suggested to occur via Ca^{2+}-dependent inhibition of K^+ channels and activation of ryanodine receptor calcium release channels (RyRs). Activation of RyR is mediated through direct binding of CE to the receptor, thus making CE a "Ca^{2+} sensor" (*3*−*6*). CE was also reported to play a role in Alzheimer's disease (*7*, *8*) although its mechanistic role in the disease is unknown. There are two variants of CE (CE_A and CE_B), with the major difference residing in the last 10 C-terminal residues. We have shown that CE_B binds three Ca^{2+} with an apparent K_d of 1 μM (*2*).

While the physiological function(s) of the SCP subfamily is (are) unclear, it has been implicated that these proteins are involved in chelation of Ca^{2+} and Mg^{2+} (for review, see ref *9*). All SCPs have four EF-hand motifs; however, only two to three are functional. Ca^{2+} binding has been preserved in the first and third EF-hands of all known SCPs. Most SCPs also have a third functional Ca^{2+} binding site, in either the second or fourth EF-hand (*9*). Crayfish and amphioxus SCPs bind three Ca^{2+}, in EF-hands I, II, and III (*10*). Another characteristic of SCPs is the presence of at least one mixed Ca^{2+}/Mg^{2+} binding site. Although SCPs were thought to occur only in muscle, they have also been detected in neurons (*11*, *12*). Using multiple sequence alignments we have shown that SCPs can be divided into a muscle group and a neuronal group (*2*). On the basis of this classification, we suggested that these two groups may have different functions; those in the neurons are Ca^{2+} sensor proteins and those in the muscle may be Ca^{2+} buffers.

To advance our understanding of the function of CE_B, we have determined the effect of Ca^{2+} and Mg^{2+} on the structure, folding, and stability of CE_B. We find that CE_B is a multidomain protein that shows complex denaturation. Under native conditions, it can adopt three distinct conformational

† This work was supported by research grants from the Canadian Institutes of Health Research (CIHR) (to A.C., M.I., and D.R.R.) and the Swiss National Science Foundation (J.A.C). Z.G. was supported by a CIHR Doctoral Research Award. M.I. is a recipient of a CIHR Scientist Award and Howard Hughes Medical Institute International Scholar Award.

* To whom correspondence should be addressed at the University Health Network, Princess Margaret Hospital, Room 7-125, 610 University Ave., Toronto, Ontario M5G 2M9, Canada. Tel: +1-416-946-2000. Fax: +1-416-946-6529. E-mail: chakrab@uhnres.utoronto.ca.

‡ Ontario Cancer Institute and University of Toronto.

§ University of Geneva.

[1] Abbreviations: ANS, 8-anilino-1-naphthalenesulfonic acid; CD, circular dichroism; CE, calexcitin; DTNB, 5,5′-dithiobis(2-nitrobenzoic acid); EGTA, ethylene glycol bis(β-aminoethyl ether)-*N*,*N*,*N*′,*N*′-tetraacetic acid; RyR, ryanodine receptor; SCP, sarcoplasmic calcium binding protein; UV, ultraviolet.

10.1021/bi034047j CCC: $25.00
Published on Web 04/15/2003

states that are dependent on the binding of Mg^{2+}/Ca^{2+}. The first state is the metal-free state in which one domain possesses putative molten globule characteristics, while the second domain is natively folded. Binding of Mg^{2+}, which induces native structure in the putative molten globule domain, produces the second state. The third conformational state is obtained by binding three Ca^{2+}- to Mg^{2+}-CE_B, displacing Mg^{2+} from the EF-hands. While both the Mg^{2+}- and Ca^{2+}-bound states have native folds, they differ in tertiary structure and thermodynamic stability. On the basis of the measured ion binding affinities and the intracellular ion concentrations, it appears that Mg^{2+}-CE_B represents the resting state and Ca^{2+}-CE_B corresponds to the active state under physiological conditions.

EXPERIMENTAL PROCEDURES

Cation Binding. All chemicals were obtained from Sigma (St. Louis, MO), unless otherwise stated. CE_B was expressed, isolated, and analyzed for purity as described previously (*2*). For cation binding experiments, all Ca^{2+} was first removed from the protein by addition of ethylene glycol bis(*β*-aminoethyl ether)-*N*,*N*,*N*′,*N*′-tetraacetic acid (EGTA) to a final concentration of 1 mM, followed by washing and concentrating the solution in 1 mM EGTA, 100 mM KCl, and 50 mM Tris-HCl (pH 7.5) using Amicon filters (Millipore, Bedford, MA) with a molecular mass cutoff of 10 kDa. Then, EGTA was removed by gel filtration on a home-packed Sephadex G-25 column that was previously treated to remove Ca^{2+} contamination and equilibrated in 100 mM KCl and 50 mM Tris-HCl (pH 7.5). Ca^{2+} binding was measured by the flow dialysis method of Colowick and Womack (*13*) at 25 °C in 100 mM KCl and 50 mM Tris-HCl (pH 7.5). Flow dialyses were carried out in 0.5 and 2 mM $MgCl_2$ and in the absence of $MgCl_2$. Binding of Mg^{2+} to CE_B, in the absence of Ca^{2+}, was measured by the equilibration gel filtration method as described previously (*14*). Measurements were taken at 25 °C in 100 mM KCl and 50 mM Tris-HCl (pH 7.5). Data processing and evaluation of binding constants were done as described previously (*15*). The effect of Mg^{2+} on the Ca^{2+} binding constants was evaluated with the competition equation $K_{Ca}/K_{Ca,app} = 1 + K_{Mg,comp}[Mg^{2+}]$, where K_{Ca} and $K_{Ca,app}$ are the binding constants in the absence and presence of Mg^{2+}, respectively, and $K_{Mg,comp}$ is the calculated Mg^{2+} binding constant in the absence of Ca^{2+}.

Thiol Reactivity. Thiol reactivity was assayed after overnight incubation of CE_B with 100 mM dithiothreitol (DTT) at pH 8.5, followed by desalting on a Sephadex G-25 column equilibrated in a nitrogen-saturated solution of 100 mM KCl and 50 mM Tris-HCl (pH 7.5). The thiol reactivity was measured spectrophotometrically (Perkin-Elmer Lambda 16) by monitoring the absorbance changes at 412 nm, which reports on the kinetics of reduction of 5,5′-dithiobis(2-nitrobenzoic acid) [DTNB; Fluka, Oakville, Ontario, Canada (*16*)].

Circular Dichroism (CD) Spectroscopy. CD measurements were made on an Aviv 62DS spectropolarimeter at room temperature. The protein was dialyzed against a solution containing 2 mM Tris-HCl (pH 7.5) and 100 mM KCl. Samples contained (a) 0.5 mM ethylenediaminetetraacetic acid (EDTA; apo-CE_B), (b) 2 mM $MgCl_2$ and 0.5 mM EGTA (Mg^{2+}-CE_B), or (c) 2 mM $CaCl_2$ (Ca^{2+}-CE_B). Protein concentrations were determined by UV absorption using an extinction coefficient (ϵ_{280}) of 49270 M^{-1} cm^{-1}, calculated by the method of Gill and von Hippel (*17*). Far-UV CD spectra were recorded in a quartz cuvette with a 0.1 cm path length, a protein concentration of 13.9 μM, and a 10 s averaging time. Near-UV spectra were recorded in a quartz cuvette with a path length of 1 cm containing a protein solution of 1.168 mg/mL. Thermal denaturation experiments were recorded at 222 nm (with 30 s equilibration time and 30 s averaging time) in a quartz cuvette with a 0.1 cm path length and a protein concentration of 0.84 mg/mL. Urea denaturation studies were recorded at 222 nm in a quartz cuvette with a 0.1 cm path length and a protein concentration of 0.84 mg/mL. In addition to the preparation of the samples described above, samples that were subjected to unfolding studies using temperature or urea contained 1 mM DTT to ensure reversibility of unfolding. Solutions containing various urea concentrations were prepared using a saturated urea solution of 10.49 M.

Fluorescence Spectroscopy. Steady-state fluorescence was measured using a Photon Technology International QM-1 spectrophotometer (London, Ontario, Canada). Samples were prepared as for the CD experiments (see above) with volumes of 0.5 mL. Experiments were performed at 25 °C. Tryptophan emission spectra were collected from 305 to 400 nm (λ_{ex} 295 nm, 10 nm/s, 10 repeats, slit width 2 nm for excitation and emission). The protein solution was 30.95 μM (as determined by UV absorption). The same samples were used for 8-anilino-1-naphthalenesulfonic acid (ANS) binding experiments. ANS emission spectra were recorded from 400 to 600 nm (λ_{ex} 372 nm, 10 nm/s, 10 repeats, slit width 2 nm for excitation and emission). Samples contained a 10-fold molar excess of ANS. Tryptophan emission spectra in the presence of urea were collected for 10 min at 343 nm (λ_{ex} 295 nm, 1 nm/s, slit width 3 nm for excitation and emission). The protein solution was 19.40 μM (as determined by UV absorption), and all samples contained 1 mM DTT.

Data Analysis. Urea denaturation curves that showed an inflection in the equilibrium unfolding transition suggest a three-state unfolding process involving a stable intermediate (I) in the unfolding of the protein from the native (N) to the unfolded (U) state. The equation describing a three-state denaturation transition (*18*) is

$$F_{app} = \frac{K_{IU}(Z_I + K_{NI})}{1 + K_{IU}(1 + K_{NI})} \quad (1)$$

where F_{app} is the apparent fraction of folded protein, Z_I normalizes the optical properties of the intermediate to those of the native and unfolded protein forms, and K_{NI} and K_{IU} are the equilibrium constants for the native to intermediate and intermediate to unfolded transitions, respectively. F_{app} values were calculated using the equation

$$F_{app} = \frac{y_{obs} - y_U}{y_N - y_U} \quad (2)$$

where y_{obs} is the observed value of the spectroscopic parameter and y_U and y_N are the values of the native and unfolded forms of the protein, respectively. On the basis of

the linear extrapolation model for chemical denaturation, eq 1 can be rewritten as

$$F_{app} = \exp[(-\Delta G_{IU}^{H_2O} + m_{IU}c)/RT] \times [Z_I + \exp[(-\Delta G_{NI}^{H_2O} + m_{NI}c)/RT]]/\{1 + \exp[(-\Delta G_{IU}^{H_2O} + m_{IU}c)/RT] \times [1 + \exp[(-\Delta G_{NI}^{H_2O} + m_{NI}c)/RT]]\} \quad (3)$$

where $\Delta G_{NI}^{H_2O}$ and $\Delta G_{IU}^{H_2O}$ are the free energy changes in the absence of denaturant for the native to intermediate and intermediate to unfolded transitions, respectively, m_{NI} and m_{IU} are cooperativity parameters of the native to intermediate and intermediate to unfolded transitions, respectively, and c is the denaturant concentration. Nonlinear least-squares fitting of eq 3 to urea denaturation curves was performed using the program SigmaPlot.

RESULTS

Measurement of the Binding Affinities of Ca^{2+} and Mg^{2+} to CE_B. On the basis of the amino acid sequence, we have previously identified four putative EF-hand motifs in CE_B, three of which were proposed to be functional. Measurements of Ca^{2+}-induced changes in tryptophan fluorescence agreed with this prediction and showed that CE_B binds three Ca^{2+} with an apparent K_d of about 1 μM. Furthermore, $^{15}N-^{1}H$ heteronuclear single-quantum correlation (HSQC) spectra indicated that Ca^{2+}-CE_B has three downfield-shifted (>10 ppm in the HN direction) peaks (*2*). These peaks are characteristic signatures of functional EF-hands and arise from the sixth residue of the Ca^{2+} binding loop of each EF-hand (*19*). Intriguingly, these data are different from those of a previous study on CE_A, which reported two functional Ca^{2+} binding sites and identified only two putative EF-hand motifs (*5*). However, the study on CE_A was done in the presence of 5 mM $MgCl_2$, which might have interfered with the results, since SCPs are known to have at least one mixed Ca^{2+}/Mg^{2+} binding site. To clarify this issue, we have now completed Ca^{2+} and Mg^{2+} binding measurements and determined their intrinsic binding constants. Figure 1A shows the Ca^{2+} binding isotherms in 0.5 and 2 mM $MgCl_2$ and in the absence of $MgCl_2$; Figure 1B shows the Mg^{2+} binding isotherm in the absence of Ca^{2+}. Table 1 summarizes the average Ca^{2+} binding affinities obtained from duplicate experiments. In the absence of Mg^{2+}, CE_B binds three Ca^{2+} with pronounced positive cooperativity (n_H) of 1.65 and intrinsic dissociation constants ranging from 0.37 to 3.3 μM, which translates to an apparent K_d of 0.77 μM. This is in excellent agreement with previously published fluorescence data and confirms that CE_B binds three Ca^{2+}, as was suggested by the amino acid sequence and HSQC spectrum (*2*). Furthermore, it is in agreement with other SCPs, as they share the characteristic pronounced positive cooperativity (*20*). To investigate the effect of Mg^{2+} on Ca^{2+} binding to CE_B, the Ca^{2+} binding measurements were repeated in the presence of 0.5 and 2 mM $MgCl_2$, the approximate range of intracellular Mg^{2+} concentration (*21*). Similar to other SCPs, the Ca^{2+} binding constants are affected by the presence of Mg^{2+}. In the presence of 0.5 mM $MgCl_2$, CE_B binds three Ca^{2+} with intrinsic dissociation constants ranging from 1.5 to 4.8 μM, which translates to an apparent K_d of 2.58 μM and has an n_H of 1.1. The decrease in the apparent Ca^{2+} binding affinity arises from a reduction in the intrinsic dissociation constants of two sites, while the third site is largely unaffected by Mg^{2+}. Again, in the presence of 2 mM Mg^{2+}, Ca^{2+} binding to one site is largely unaffected by the presence of Mg^{2+}, whereas the other two sites show reductions in their Ca^{2+} affinities. If we assume that the Mg^{2+}-induced decrease in the two last binding steps is due

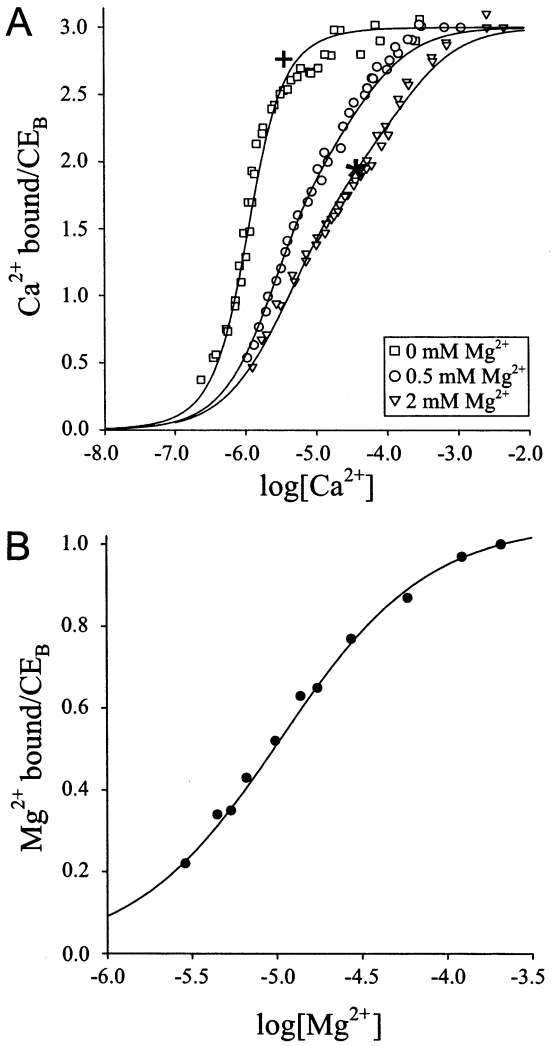

FIGURE 1: (A) Direct Ca^{2+} binding to CE_B monitored by flow dialysis at 25 °C in 50 mM Tris-HCl, pH 7.5, and 100 mM KCl containing 0 (□), 0.5 mM (○), or 2 mM $MgCl_2$ (▽). The protein concentration is 25 μM. Equilibrium gel filtration of CE_B in the absence (+) and presence of 2 mM Mg^{2+} (*) is also shown. (B) Direct Mg^{2+} binding to CE_B monitored with equilibrium gel filtration at room temperature in 50 mM Tris-HCl, pH 7.5, 100 mM KCl, and 50 μM EGTA and various Mg^{2+} concentrations.

Table 1: Summary of the Intrinsic Ca^{2+} Binding Constants (in M^{-1}) of CE_B in the Presence of Various Mg^{2+} Concentrations (in M^{-1})

	Mg^{2+}			
	0 mM	0.5 mM	2 mM	$K'_{Mg,comp}$[a]
K_{a1}	3.0×10^5	2.1×10^5	1.9×10^5	$\sim 4 \times 10^2$
K_{a2}	9.1×10^5	3.0×10^5	1.0×10^5	4.0×10^3
K_{a3}	2.7×10^6	6.5×10^5	1.6×10^4	8.5×10^4

[a] Calculated with the competition equation $K'_{Ca}/K'_{Ca,app} = 1 + K'_{Mg,comp}[Mg^{2+}]$, where K'_{Ca} is the intrinsic constant in the absence of Ca^{2+}, $K'_{Ca,app}$ is the apparent constant in the presence of Mg^{2+}, and $K'_{Mg,comp}$ is the calculated constant for Mg^{2+} in the absence of Ca^{2+}.

Table 2: Summary of Thiol Reactivity of Various Forms of CE_B[a]

	apo-CE_B	Mg^{2+}-CE_B	Ca^{2+}-CE_B
Cys_1	<1 s[b] very rapid	<1 s very rapid	~10 s moderately fast
Cys_2	~10 s moderately fast	~10 s moderately fast	~200 s slow
Cys_3	~10 s moderately fast	~200 s slow	nonreactive
Cys_4	~200 s slow	nonreactive	nonreactive

[a] The numbers indicate the order of thiol reactivity rather than a specific Cys residue. [b] The values correspond to estimated half-life times ($t_{1/2}$).

to competition, $K_{Mg,comp}$ values of 4×10^3 and 8.5×10^4 M^{-1} are obtained (Table 1, last column). These results are consistent with the possibility that CE_B has one Ca^{2+}-specific binding site, and two mixed Ca^{2+}/Mg^{2+} binding sites. Of the mixed sites, one is very sensitive to Mg^{2+}, whereas the other one displays a weak Mg^{2+} effect. This is reminiscent of amphioxus (*22*) and crayfish (*10*) SCPs. Further evidence for this model is provided by the finding obtained from equilibrium gel filtration that CE_B binds 1.95 Ca^{2+} in the presence of 2 mM Mg^{2+} and 38 μM Ca^{2+} (black star in Figure 1A).

The experiments presented above suggest that there is a strong interaction between CE_B and Mg^{2+}. To obtain a direct measurement of the Mg^{2+} binding constant, equilibrium gel filtration was used and revealed a single high-affinity site with a K_d of 11 μM ($K_{Mg} = 9.1 \times 10^4$ M^{-1}). This dissociation constant is in excellent agreement with that obtained from the competition equation (see Experimental Procedures; $K_d = 12$ μM). The second, low-affinity ($K_{Mg} < 4 \times 10^3$ M^{-1}) Mg^{2+} binding site could not be detected by the equilibrium gel filtration method. The Mg^{2+} binding affinity of the high-affinity site in CE_B is similar to that of troponin C (*23*), parvalbumin (*24*), and SCP from crayfish (*20*), sandworm (*25*), and amphioxus (*26*), all of which have a K_d for Mg^{2+} at around 25 μM. This finding also suggests that Mg^{2+} binding may have an evolutionary significance.

Thiol Reactivity as a Probe of Ion Binding to CE_B. CE_B contains four Cys residues: Cys_{24} and Cys_{42} located in EF-I, Cys_{93} located in EF-II, and Cys_{145} located in EF-IV (*2*). Given that the Cys residues lie within the EF-hands, it is conceivable that their reactivity would change upon binding Ca^{2+} and/or Mg^{2+}. This change may result from ion binding causing either steric hindrance or conformational change. Thiol reactivity experiments were conducted using metal-free (apo-CE_B), Mg^{2+}-bound (Mg^{2+}-CE_B) and Ca^{2+}-bound (Ca^{2+}-CE_B) protein. As seen in Table 2, all Cys are reactive in apo-CE_B, with one reacting very rapidly, with a half-life time ($t_{1/2}$) less than 1 s, two reacting moderately fast ($t_{1/2}$ ~10 s), and one reacting slowly ($t_{1/2}$ ~200 s). In Mg^{2+}-CE_B, one of the moderately fast reacting Cys becomes nonreactive, i.e., completely inaccessible to DTNB. In Ca^{2+}-CE_B, two Cys are affected: the very rapidly reacting and one moderately fast reacting Cys become nonreactive. These data suggest that in CE_B there are three states with distinct thiol reactivities: the state of the apo-, Mg^{2+}-, and Ca^{2+}-CE_B. All CE_B forms contain a slow-reacting Cys; it is possible that this Cys is part of EF-IV, which is predicted to be nonfunctional (*2*) and hence unaffected by ion binding. However, the present data cannot be used to assign the identity of the moderate- or fast-reacting Cys.

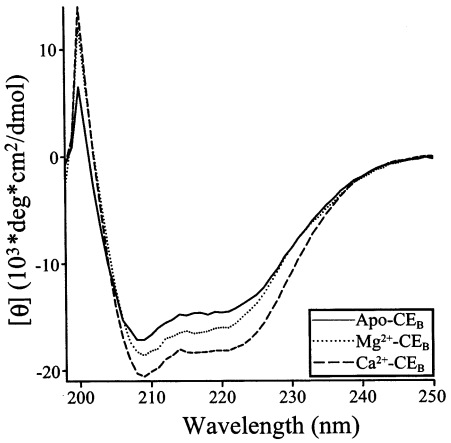

FIGURE 2: Far-UV circular dichroism spectra of CE_B. There are minor spectral changes upon the addition of Ca^{2+} or Mg^{2+}. The $[\theta]_{208}$ value is more negative than the $[\theta]_{222}$ value, atypical of the canonical α-helical protein (*53*) but consistent with other SCPs (*26*, *54*, *55*).

Ion-Induced Changes in Secondary and Tertiary Structure of CE_B Monitored by Circular Dichroism. The far-UV CD spectra of apo-CE_B, Mg^{2+}-CE_B, and Ca^{2+}-CE_B are shown in Figure 2. The spectra of all CE_B forms are indicative of a predominantly α-helical protein with characteristic CD bands at 208 and 222 nm. There are slight differences in the far-UV CD spectra of this protein, which we attribute to rearrangement of secondary structure rather than a change in the content of secondary structure. Similar phenomena have been observed in other SCPs. The $[\theta]_{222}$ of metal-free forms of scallop SCP increased upon Mg^{2+} binding and increased further upon Ca^{2+} binding (*27*). Ca^{2+}-induced changes in the far-UV CD spectrum of the EF-hand protein troponin C were shown to be caused by changes in the orientation of the preexisting α-helices rather than a change in helix content (*28*).

Unlike the far-UV CD spectra, the near-UV CD spectra of CE_B show dramatic differences (Figure 3). The near-UV CD spectrum of apo-CE_B shows several low-intensity CD bands, which can be attributed to the abundant Trp, Tyr, and Phe in the protein. Addition of Mg^{2+} to produce Mg^{2+}-CE_B causes a dramatic increase in the magnitude of the CD bands, with the most pronounced change occurring in the Trp bands at 280 and 290 nm. Addition of Ca^{2+} to apo-CE_B to produce Ca^{2+}-CE_B causes an equally dramatic change in the near-UV CD spectrum; however, in this instance the change is in the opposite direction with the development of a prominent Trp CD band at 292 nm with negative ellipticity. These results indicate that CE_B exists in three distinct conformational states that can be interconverted by the addition of Mg^{2+}/Ca^{2+}. Apo-CE_B and Mg^{2+}-CE_B comprise the first and second states, respectively, while Ca^{2+}-CE_B corresponds to the third conformational state.

It should be noted that the magnitudes of near-UV CD bands of apo-CE_B are lower than those observed in our previous study (*2*). We have determined that this difference is due to the 100 mM KCl used in the present study. Upon removal of KCl, the intensity of the bands was restored (data not shown).

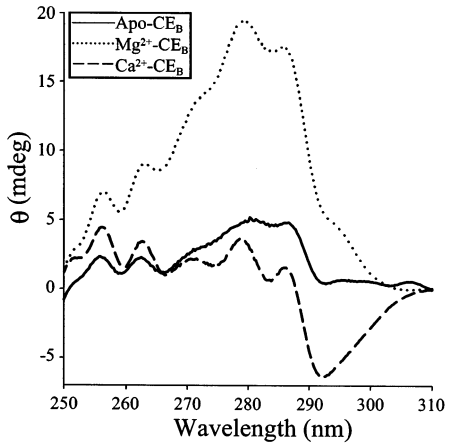

FIGURE 3: Near-UV circular dichroism spectra of CE_B. There are approximately seven peaks in the spectra of CE_B in the absence of metals and in the presence of Mg^{2+} and Ca^{2+}, due to an abundance of aromatic residues within the amino acid sequence. The spectrum indicates that the protein undergoes a conformational change upon Mg^{2+} binding. Similarly, there is also a Ca^{2+}-induced conformational change, as reported previously (*2*).

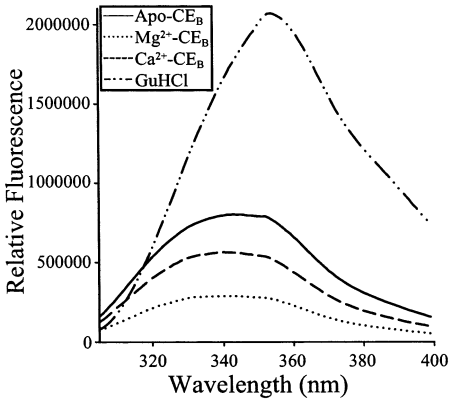

FIGURE 4: Tryptophan fluorescence emission spectra of CE_B. There is a reduction in the fluorescence intensity of nearly 60% in the signal of apo-CE_B as compared to denatured CE_B. This is also accompanied by a 10 nm blue shift of the maxima of the folded CE_B species relative to the unfolded CE_B. Relative to apo-CE_B, there is a fluorescence intensity decrease of nearly 65% upon Mg^{2+} binding and about 30% upon Ca^{2+} binding (see also ref *2*) to CE_B. These data suggest that CE_B undergoes a conformational change in the presence of Ca^{2+} or Mg^{2+} involving the chemical environment of some, if not all, Trp residues.

Ion-Induced Changes in Intrinsic Trp Fluorescence of CE_B. As stated above, the near-UV CD bands of Trp residues display the largest changes upon metal binding. We have also examined whether metal binding induces similar effects on intrinsic Trp fluorescence of CE_B. Figure 4 shows the intrinsic Trp fluorescence of various forms of CE_B. While CE_B unfolded in 6 M guanidine hydrochloride (GuHCl) has the greatest intrinsic fluorescence with a maximum at 354 nm, folded apo-CE_B shows a lower magnitude of Trp fluorescence with a maximum at 343 nm. This suggests that in the folded state the Trp fluorescence is quenched. Mg^{2+} binding to CE_B causes further quenching, resulting in a 65% decrease in signal intensity. Addition of Ca^{2+} to apo-CE_B relieves some of the Mg^{2+}-induced quenching, with Ca^{2+}-CE_B having an intrinsic fluorescence midway between that of apo-CE_B and Mg^{2+}-CE_B. The intrinsic Trp fluorescence data parallel the near-UV CD data, reinforcing the suggestion of the presence of three distinct conformational states. As

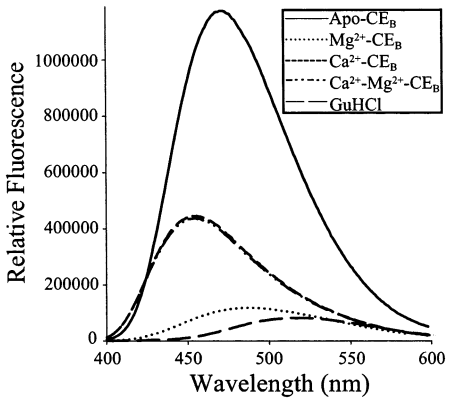

FIGURE 5: ANS binding of CE_B. There is a 12-fold increase in the fluorescence intensity of apo-CE_B as compared to denatured CE_B. This is also accompanied by a 50 nm blue shift of the maximum of apo-CE_B. Relative to apo-CE_B, there is a fluorescence intensity decrease of nearly 90% upon Mg^{2+} binding and about 60% upon Ca^{2+} binding to CE_B. The maxima relative to apo-CE_B experience a 15 nm red shift and a 15 nm blue shift, respectively. There is no observable difference between CE_B in the presence of 2 mM $CaCl_2$ alone (Ca^{2+}-CE_B) or in the presence of 2 mM $CaCl_2$ and 2 mM $MgCl_2$ (Ca^{2+}-Mg^{2+}-CE_B).

stated above, the first state is that of apo-CE_B, the second state is that of Mg^{2+}-CE_B, and the third conformational state is that of Ca^{2+}-CE_B.

Interestingly, both scallop and sandworm SCP show somewhat similar effects of Ca^{2+}/Mg^{2+} binding on Trp fluorescence. In scallop SCP, both Mg^{2+} and Ca^{2+} caused a decrease in Trp fluorescence; however, the decrease seen with Ca^{2+} was greater (*27*). In sandworm SCP, the Trp fluorescence profile of the various protein forms looks remarkably similar to that observed with CE_B. However, the ions cause an increase in fluorescence rather than a decrease as seen with CE_B. Nevertheless, the change seen in the presence of Mg^{2+} differs from the change that occurs in the presence of Ca^{2+} (*25*). Therefore, as presented above, CE_B and SCPs in general display three distinct structures based on the type of ion that is bound to the protein.

Ion-Induced Native vs Non-Native Conformational States of CE_B Probed by ANS Fluorescence. Precheur et al. (*29*) showed that sandworm SCP is a molten globule in the metal-free state. To determine if CE_B also displays a similar characteristic, ANS binding to the protein was investigated. An enhancement of fluorescence accompanies binding of ANS to exposed hydrophobic regions of a protein and is a probe of non-native conformational states, such as molten globules (*30*). As presented in Figure 5, denatured CE_B shows little ANS binding, while folded apo-CE_B shows a dramatic increase in ANS binding, suggesting that CE_B has increased hydrophobic exposure in the absence of any metals. Moreover, the ANS binding study revealed further insights into the basic properties of CE_B. As seen in Figure 5, Mg^{2+}-CE_B shows very little ANS binding, indicating that it is a tightly packed protein with very few exposed hydrophobic patches. Addition of Ca^{2+} to apo-CE_B produces a conformational state that displays ANS binding. These results are in agreement with the near-UV CD and intrinsic Trp fluorescence data, which suggest the presence of three distinct conformational states of CE_B.

The ANS binding site(s) in Ca^{2+}-CE_B is (are) different from the binding site(s) in apo-CE_B. The wavelength of

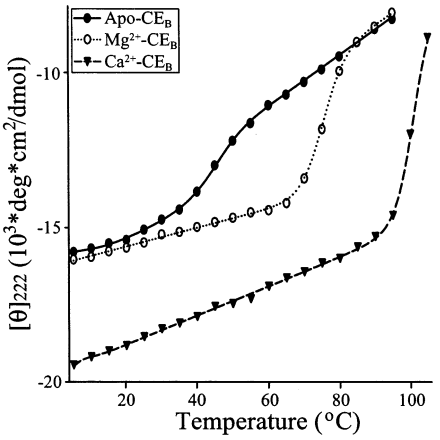

FIGURE 6: Thermal denaturation of CE_B monitored by CD. Apo-CE_B shows a weakly cooperative denaturation curve with a melting temperature (T_m) of 43.2 °C. The denaturation curve of Mg^{2+}-CE_B shows an increase in the cooperativity of unfolding and an increase in stability producing a T_m of 75.1 °C. Ca^{2+} binding to CE_B causes a dramatic increase in protein stability with a T_m of >100 °C. The melting of all three forms was fully reversible in the presence of DTT.

maximum fluorescence of apo-CE_B is 471 nm, while that of Ca^{2+}-CE_B is 452 nm. This suggests that the ANS binding site(s) in Ca^{2+}-CE_B is (are) less water accessible than that of apo-CE_B. This is consistent with the finding that Ca^{2+}-CE_B does not bind to phenyl-Sepharose (data not shown), which is a useful probe for Ca^{2+} sensor proteins (*31*). Therefore, the hydrophobic binding site displays specificity for hydrophobic ligands and suggests that the hydrophobic pocket is a well-defined groove rather than an exposed hydrophobic patch. The ANS fluorescence of CE_B in the presence of 2 mM $CaCl_2$ and 2 mM $MgCl_2$ is identical to that of CE_B in 2 mM $CaCl_2$ alone, indicating that the ANS binding site in Ca^{2+}-CE_B is unaffected by the addition of Mg^{2+} (Figure 5).

Thermal Denaturation of CE_B Monitored by CD. In addition to the structural differences among apo-, Mg^{2+}-, and Ca^{2+}-CE_B, there are also great differences in folding and stability of these conformational states. Thermal denaturation of apo-CE_B monitored by far-UV CD (Figure 6) revealed a weakly cooperative denaturation curve with a melting temperature (T_m) of 43.2 °C. Addition of Mg^{2+} to produce Mg^{2+}-CE_B has two major effects: an increase in stability producing a T_m of 75.1 °C and an increase in the cooperativity of unfolding. Taken together, the results of near-UV CD (Figure 3), ANS binding (Figure 5), and thermal denaturation experiments indicate that Mg^{2+} binding increases global stability. Ca^{2+} binding to apo-CE_B causes a dramatic increase in the stability of Ca^{2+}-CE_B, with a T_m of >100 °C. The melting of all three forms was fully reversible in the presence of DTT; however, in the absence of the reducing agent, refolding of apo-CE_B is not reversible.

Urea Denaturation of CE_B Monitored by CD and Intrinsic Trp Fluorescence. Unlike thermal denaturation, urea denaturation of apo-CE_B monitored by CD shows a distinct inflection point separating two unfolding phases (Figure 7A). This indicates that unfolding of CE_B is not a two-state process and suggests that CE_B is at least a two-domain protein in which the individual domains differ in stability and unfold independently. The denaturation midpoint of the first domain of apo-CE_B occurs near 1.75 M urea, while the second

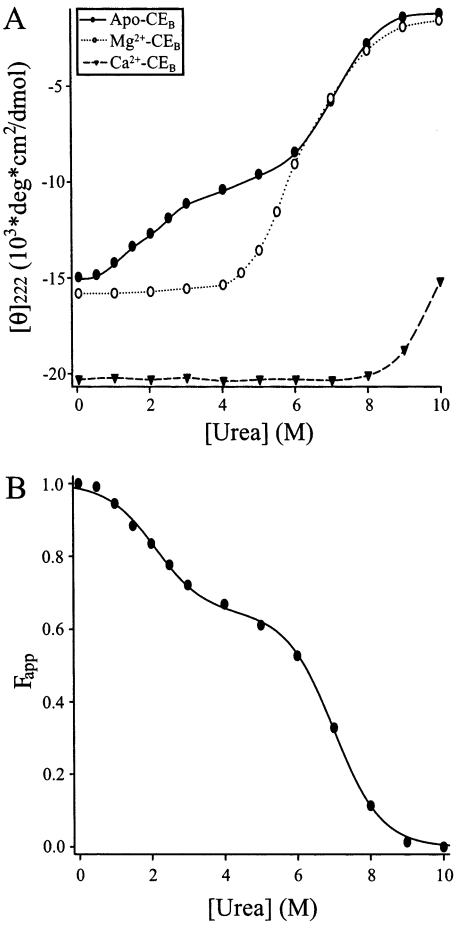

FIGURE 7: Urea denaturation of CE_B monitored by CD. (A) Denaturation of apo-CE_B shows a distinct inflection point separating two unfolding phases, indicating that this is not a two-state process and that CE_B is at least a two-domain protein. The denaturation curve of Mg^{2+}-CE_B differs greatly with the first phase of the apo-CE_B curve; however, the curve of Mg^{2+}-CE_B superimposes on the second phase of the apo-CE_B curve, suggesting that Mg^{2+} binding stabilizes the putative molten globule domain but not the native domain. The denaturation curve of Ca^{2+}-CE_B shows that this form is very stable and resistant to unfolding and suggests that Ca^{2+} stabilizes both the putative molten globule and native domains of CE_B. (B) The denaturation curve of apo-CE_B was fit to a three-state model. On the basis of this fit, the following values (±standard error) were obtained for apo-CE_B: $\Delta G_{NI}^{H_2O} = -1.89 \pm 0.153$ kcal/mol, $m_{NI} = 0.891 \pm 0.087$ kcal/mol^2, $\Delta G_{IU}^{H_2O} = -6.41 \pm 0.475$ kcal/mol, $m_{IU} = 0.917 \pm 0.064$ kcal/mol^2, and $Z_I = 0.645 \pm 0.015$. On the basis of the calculated free energy changes, the intermediate state is energetically more similar to the native state than the unfolded state.

domain has a midpoint near 7.5 M urea. The denaturation curve was fit to a three-state model as described above. On the basis of this fit (Figure 7B), the following values (±standard error) were obtained for apo-CE_B: $\Delta G_{NI}^{H_2O} = -1.89 \pm 0.153$ kcal/mol, $m_{NI} = 0.891 \pm 0.087$ kcal/mol^2, $\Delta G_{IU}^{H_2O} = -6.41 \pm 0.475$ kcal/mol, $m_{IU} = 0.917 \pm 0.064$ kcal/mol^2 and $Z_I = 0.645 \pm 0.015$. On the basis of the calculated free energy changes, the intermediate state is energetically more similar to the native state than the unfolded state.

While the urea denaturation curve of Mg^{2+}-CE_B differs greatly from the first phase of the apo-CE_B denaturation curve, the unfolding curve of Mg^{2+}-CE_B superimposes on the second phase of the apo-CE_B denaturation curve (Figure

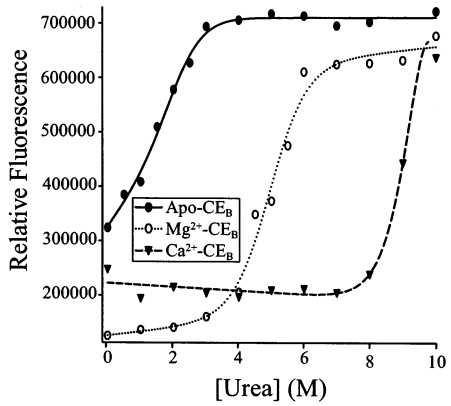

FIGURE 8: Urea denaturation of CE_B monitored by intrinsic tryptophan fluorescence. Apo-CE_B appears partially unfolded even in the absence of urea and becomes completely unfolded by 3 M urea. The urea denaturation curve of Mg^{2+}-CE_B has well-defined baselines and a cooperative transition. Ca^{2+}-CE_B shows very high stability and is resistant to urea unfolding.

7A). This suggests that Mg^{2+} binding stabilizes one domain but not the other. The urea denaturation curve of Mg^{2+}-CE_B was not typical of a two-state transition (see below). Paralleling the thermal denaturation experiment (Figure 6), Ca^{2+}-CE_B is very stable and resistant to urea-induced unfolding (Figure 7A). Interestingly, Ca^{2+} binding, unlike Mg^{2+} binding, stabilizes both domains.

We have also studied the urea unfolding of the CE_B forms using intrinsic Trp fluorescence. As seen in Figure 8, apo-CE_B appears partially unfolded even in the absence of urea, continues to unfold with increasing urea concentrations, and becomes completely unfolded by 3 M urea. This transition correlates with the first phase of the urea denaturation curve of apo-CE_B monitored by CD (Figure 7A). Therefore, Trp fluorescence reports on the unfolding of the less stable domain of apo-CE_B. It is interesting to note that CE_B has five Trp in the N-terminal half and only two Trp in the C-terminal half (*2*). The urea denaturation curve of Mg^{2+}-CE_B determined by Trp fluorescence (Figure 8) is similar to the curve determined by CD (Figure 7A) in that they both have well-defined baselines and a cooperative transition. However, the denaturation midpoint is different when measured with these methods: 5 M urea for the tryptophan fluorescence curve (Figure 8) and 6 M urea for the CD curve (Figure 7A). This difference in denaturation midpoints indicates that the unfolding of Mg^{2+}-CE_B is a not a two-state process and provides further evidence that CE_B is composed of at least two domains that unfold independently. However, both the CD and the fluorescence denaturation curves of Mg^{2+}-CE_B did not show a clear deflection point of a three-state transition. Consequently, the absence of an inflection point in the denaturation curves of Mg^{2+}-CE_B precluded fitting of the data to a three-state model. As seen in the thermal denaturation experiment (Figure 6) and the urea denaturation data obtained by CD (Figure 7A), Ca^{2+}-CE_B shows very high stability and is resistant to urea unfolding as monitored by intrinsic Trp fluorescence (Figure 8).

DISCUSSION

The characteristic features of SCPs are molecular weights around 22 kDa, the presence of two or three functional EF-hands and one or two nonfunctional EF-hands, and at least one mixed Ca^{2+}/Mg^{2+} binding site. Our past work (*2*) established that CE_B is a member of the SCP subfamily and contains four EF-hands: a nonfunctional site IV, one Ca^{2+}-specific site, and two mixed Ca^{2+}/Mg^{2+} binding sites but with very different affinities for Mg^{2+}. This binding pattern is very similar to that of amphioxus SCP (*22*) and to a slightly lesser extent to the well-studied crayfish SCP (*10*, *20*). SCPs have been proposed to be Ca^{2+} buffer proteins that attenuate free Ca^{2+} concentrations after Ca^{2+} influx induced by extracellular signals (*9*). The role of Mg^{2+} in SCP function is not established, but in stimulated cells, significant amounts of Mg^{2+} are liberated upon Ca^{2+} binding to the mixed Ca^{2+}/Mg^{2+} binding sites (*32*).

Mg^{2+} is the most prevalent ion in the cytoplasm and is essential in many cellular events, such as muscle contraction, cell growth, and as a cofactor in numerous ion channels and enzymes, especially those in phosphoryl-transfer processes (for review see ref *33*). The Mg^{2+} gradient across the plasma membrane is modest, with a slightly higher concentration in the extracellular medium. Influx of Mg^{2+} occurs through passive diffusion from the extracellular space; however, efflux is through the Na^+/Mg^{2+} antiporter (*34*−*36*). Mg^{2+} is also important for normal neurological function and was shown to be neuroprotective (e.g., ref *37*). It has been used in the treatment of seizures due to hypertension (*38*, *39*) and was shown to be useful in reducing the risk of cerebral palsy and mental retardation (*40*). Furthermore, the RyR, a target of CE (*3*, *6*), is regulated by Mg^{2+} as well as Ca^{2+} (*41*, *42*). It appears that Mg^{2+} has a complementary role to Ca^{2+} in that it modulates Ca^{2+} signaling pathways. Mg^{2+} plays a regulatory role in the control of Ca^{2+} uptake, homeostasis, and release (*43*). The Ca^{2+}/Mg^{2+} ratio plays a role in regulation of plasma membrane excitability and ion channel permeability (*44*). Interestingly, Mg^{2+} also plays a role in K^+ channel inhibition (*45*, *46*), another target of CE (*3*, *5*).

In the present study, we have shown that CE_B is composed of at least two separate domains. In apo-CE_B, one domain is much less stable than the other domain. In Mg^{2+}-CE_B the unstable domain becomes natively folded and stabilized, while the other domain remains largely unaffected. Ca^{2+} binding stabilizes both domains of CE_B. Mg^{2+} binding experiments indicated the presence of two physiologically significant binding sites that differed greatly in affinity (K_d = 12−250 μM). Since Mg^{2+} binding was shown not to stabilize the natively folded domain, both Mg^{2+} binding sites apparently reside on the unstable domain. Further evidence that the unstable domain harbors the Mg^{2+} binding sites comes from near-UV CD (Figure 3) and ANS binding (Figure 5) experiments, which show induction of near-UV CD bands and reduction in ANS binding coinciding with Mg^{2+} binding.

The conformation of Mg^{2+}-CE_B is different from that of Ca^{2+}-CE_B, which adopts the third conformational state. This third state possesses a diagnostic negative near-UV CD band at 292 nm and ANS binding properties suggestive of a hydrophobic pocket. The Ca^{2+} and Mg^{2+} binding experiments revealed that while CE_B contains four EF-hand motifs (*2*), only three are functional with dissociation constants for Ca^{2+} ranging from 0.37 to 10 μM, which are typical of Ca^{2+} sensor proteins (*31*). One of the EF-hands is a typical mixed $Ca^{2+}/$

Mg^{2+} binding site, another EF-hand displays a weak Mg^{2+} antagonism, and the third EF-hand is a typical Ca^{2+}-specific site. The two EF-hands that can interact with Ca^{2+}/Mg^{2+} must both reside within the unstable domain, because Mg^{2+} binding had no effect on the stability of the native domain. Therefore, the Ca^{2+}-specific EF-hand must reside in the native domain, thus accounting for the Ca^{2+}-induced stabilizations of both domains of CE_B seen in the urea denaturation experiment monitored by CD (Figure 7A).

As noted by Nakayama and Kretsinger (*47*), most EF-hand domains have a 1000-fold higher affinity for Ca^{2+} than for Mg^{2+}. However, the intracellular Mg^{2+} concentration is in the 0.5−2 mM range (*21*), whereas the intracellular Ca^{2+} concentration ranges from nanomolar in quiescent cells to micromolar in stimulated cells (*31*). Therefore, at resting state some EF-hand domains may be occupied by Mg^{2+} but convert to a Ca^{2+}-bound form upon cell stimulation (*47*). On the basis of our measured values for the dissociation constants for Ca^{2+} and Mg^{2+} and the intracellular concentrations of these ions in quiescent cells (*47*), it is predicted that CE_B in these cells would be Mg^{2+} bound and adopt the Mg^{2+}-CE_B conformational state. The cytoplasmic concentrations of apo-CE_B and Ca^{2+}-CE_B would be negligible in quiescent cells. During Ca^{2+} influx, when intracellular Ca^{2+} levels are at their highest, the third conformational state forms. In this state, assuming a free Mg^{2+} concentration of 0.5 mM, two EF-hand motifs are filled with Ca^{2+} and the third EF-hand motif is about 70−90% occupied by Ca^{2+} and the remainder by Mg^{2+}. Accompanying the changes in metal binding state there are changes in protein conformation. Conversion of the putative resting state (i.e., Mg^{2+}-CE_B) to the putative active state (i.e., Ca^{2+}-CE_B) induces the formation of a hydrophobic pocket that can bind ANS. This hydrophobic pocket differs from the ANS binding site(s) of apo-CE_B in that ANS bound to Ca^{2+}-CE_B has a λ_{max} that is blue shifted by 17 nm from that of apo-CE_B. We speculate that this hydrophobic pocket may represent a potential target binding domain, where the RyR and K^+ channel bind. The inability of Ca^{2+}-CE_B to bind to phenyl-Sepharose is divergent from other Ca^{2+}-loaded EF-hand-containing Ca^{2+} sensors (*31*), suggesting that the hydrophobic pocket of Ca^{2+}-CE_B is more recessed than the hydrophobic target binding site of other Ca^{2+} sensors [e.g., calmodulin (*48*)]. Both apo- and Ca^{2+}-SCP from sandworm also bind ANS; however, their values of λ_{max} were identical and not blue shifted as ANS bound to Ca^{2+}-CE_B. Thus, the sandworm SCP does not a have a recessed hydrophobic pocket like Ca^{2+}-CE_B.

The Ca^{2+}/Mg^{2+} binding specificity of individual EF-hands can be tentatively assigned through comparison of the amino acid sequences of the EF-hands of CE_B with previously published mutagenesis data. EF-I contains an Asp residue at the $-Z$ ion coordination position, while EF-II and EF-III contain Glu at this position (*2*). Asp to Glu substitution at the $-Z$ position has been shown to abolish Mg^{2+} binding but retain Ca^{2+} binding (*55*), making Asp occupancy at the $-Z$ position an indicator of a mixed Ca^{2+}/Mg^{2+} binding site. Therefore, EF-I is likely to be the mixed Ca^{2+}/Mg^{2+} binding site. Since millimolar concentrations of Mg^{2+} affect the unstable domain and not the natively structured domain of CE_B (Figure 7A) and since EF-hands pair sequentially (*47*), it is likely that the unstable domain is comprised of the Mg^{2+}-sensitive EF-hands: EF-I, the mixed Ca^{2+}/Mg^{2+} binding site, and EF-II, the Ca^{2+} binding site with weak Mg^{2+} antagonism. The natively structured domain of CE_B contains EF-III and EF-IV of which EF-III is the Ca^{2+}-specific site and, as presented earlier, EF-IV is a nonfunctional site due to the lack of conservation of residues involved in ion coordination (*2*).

With regard to the structure of apo-CE_B, it is possible that the unstable domain either possesses non-native structure or is an equilibrium mixture of interconverting native and unfolded conformations. If the unstable domain is a mixture of unfolded and native conformations, the first phase of the biphasic unfolding transition of apo-CE_B would be the complete unfolding of the unstable domain and the second phase would be the unfolding of the native domain. The increase in ANS fluorescence may be caused by the exposure of a hydrophobic interdomain interface. The Mg^{2+} binding sites reside in the unstable domain; hence Mg^{2+} binding stabilizes the unstable domain and has no effect on the native domain. Ca^{2+} binding stabilizes both domains, each of which contain Ca^{2+} binding sites.

There is also experimental evidence which suggests that the unstable domain possesses non-native molten globule structure. Our previous nuclear magnetic resonance (NMR) heteronuclear single-quantum correlation (HSQC) spectrum of apo-CE_B contains many resolvable $^{15}N-HN$ cross-peaks (*2*), indicating the presence of some native structure. Additionally, the far-UV CD spectra (Figure 2) of apo-, Mg^{2+}-, and Ca^{2+}-CE_B indicate the presence of nearly identical secondary structure content. However, the near-UV CD (Figure 3) suggests that apo-CE_B lacks tertiary structure. Furthermore, the broad thermal denaturation of apo-CE_B (Figure 6) is consistent with the presence of molten globule structure (*49*). The retention of secondary structure and loss of tertiary structure taken together with the increased ANS binding and broad, noncooperative thermal denaturation are all suggestive of the presence of molten globule structure in the unstable domain.

If the unstable domain was a mixture of unfolded and native conformations in apo-CE_B, then it is likely that the HSQC spectrum of apo-CE_B would contain extra $^{15}N-HN$ cross-peaks, but this was not observed (*2*). In addition, a mixture of unfolded and native conformations for the unstable domain should result in a significant decrease in secondary structure, leading to a reduced magnitude of far-UV CD bands, but this is not the case (Figure 2). Furthermore, the three-state analysis of apo-CE_B unfolding (Figure 7B) indicates a large energetic difference of 1.9 kcal/mol between the native and intermediate states. Such a free energy difference indicates that the population of molecules with unfolded unstable domains is small under native conditions. There is evidence that sandworm SCP is also a molten globule in the metal-free state and forms a native structure upon binding the first Ca^{2+} (*29*, *50*). The Ca^{2+}/Mg^{2+}-induced conformational changes seen in CE_B are reminiscent of those in troponin C, where the role of Ca^{2+}/Mg^{2+} binding sites is to maintain the native structure of the protein, while the Ca^{2+} specific sites play a regulatory role in Ca^{2+} signaling (*51*, *52*). This evidence, therefore, reinforces the idea that apo-CE_B contains a molten globule domain and a natively folded domain which fold independently. However, further experiments are required to prove this possibility.

In conclusion, CE_B possesses two structural domains that can unfold independently and display dynamic changes induced by Ca^{2+} and Mg^{2+} binding. CE_B can exist in three conformational states: a putative molten globule state and two structurally distinct native states. The putative molten globule state seen with apo-CE_B contains one domain with molten globule characteristics and another domain with native structure. This state is unlikely to be populated in the cytoplasm. Mg^{2+} binding to the molten globule domain of apo-CE_B induces the formation of a compact, well-defined native structure and represents the first native state of the protein. This protein state is probably the most populated conformation in the cytoplasm of quiescent neurons. It is plausible that the function of the Ca^{2+}/Mg^{2+} site(s) is to prevent the protein from adopting the molten globule state and being catabolized by the proteasome. Conversely, in activated neurons the level of intracellular Ca^{2+} increases and the cell becomes highly populated with Ca^{2+}-CE_B. This second native state appears to have an exposed hydrophobic pocket, which could potentially interact with targets, such as the RyR and K^+ channel. While it is apparent that both Mg^{2+} and Ca^{2+} maintain the native structure of CE_B under physiological conditions, Ca^{2+} is the switch that activates the protein, whereas Mg^{2+} plays a structural role and maintains the native state of the inactive protein.

REFERENCES

1. Kretsinger, R. H., and Nockolds, C. E. (1973) *J. Biol. Chem. 248*, 3313−3326.
2. Gombos, Z., Jeromin, A., Mal, T. K., Chakrabartty, A., and Ikura, M. (2001) *J. Biol. Chem. 276*, 22529−22536.
3. Alkon, D. L., Nelson, T. J., Zhao, W., and Cavallaro, S. (1998) *Trends Neurosci. 21*, 529−537.
4. Nelson, T. J., Collin, C., and Alkon, D. L. (1990) *Science 247*, 1479−1483.
5. Nelson, T. J., Cavallaro, S., Yi, C. L., McPhie, D., Schreurs, B. G., Gusev, P. A., Favit, A., Zohar, O., Kim, J., Beushausen, S., Ascoli, G., Olds, J., Neve, R., and Alkon, D. L. (1996) *Proc. Natl. Acad. Sci. U.S.A. 93*, 13808−13813.
6. Nelson, T. J., Zhao, W. Q., Yuan, S., Favit, A., Pozzo-Miller, L., and Alkon, D. L. (1999) *Biochem. J. 341*, 423−433.
7. Kim, C. S., Han, Y. F., Etcheberrigaray, R., Nelson, T. J., Olds, J. L., Yoshioka, T., and Alkon, D. L. (1995) *Proc. Natl. Acad. Sci. U.S.A. 92*, 3060−3064.
8. Etcheberrigaray, E., Gibson, G. E., and Alkon, D. L. (1994) *Ann. N.Y. Acad. Sci. 747*, 245−255.
9. Hermann, A., and Cox, J. A. (1991) *Comp. Biochem. Physiol. 111B*, 337−345.
10. Wnuk, W., Cox, J. A., Kohler, L. G., and Stein, E. A. (1979) *J. Biol. Chem. 254*, 5284−5289.
11. Kelly, L. E., Phillips, A. M., Delbridge, M., and Stewart, R. (1997) *Insect Biochem. Mol. Biol. 27*, 783−792.
12. Pauls, T. L., Cox, J. A., Heizmann, C. W., and Hermann, A. (1993) *Eur. J. Neurosci. 5*, 549−559.
13. Colowick, S. P., and Womack, F. C. (1969) *J. Biol. Chem. 244*, 774−777.
14. Durussel, I., Mehul, B., Bernard, D., Schmidt, R., and Cox, J. A. (2002) *Biochemistry 41*, 5439−5448.
15. Cox, J. A. (1996) in *Guidebook to the Calcium-Binding Proteins* (Celio, M. R., Pauls, T. L., and B., S., Eds.) p 238, Sambrook & Tooze Publication at Oxford University Press, Oxford.
16. Riddles, P. W., Blakeley, R. L., and Zerner, B. (1983) *Methods Enzymol. 91*, 49−60.
17. Gill, S. C., and von Hippel, P. H. (1989) *Anal. Biochem. 182*, 319−326.
18. Finn, B. E., Chen, X., Jennings, P. A., Saalau-Bethell, S. M., and Matthews, C. R. (1992) in *Protein Engineering* (Rees, A. R., Sternberg, M. J. E., and Wetzel, R., Eds.) pp 167−189, Oxford University Press, Oxford.
19. Ikura, M., Minowa, O., and Hikichi, K. (1985) *Biochemistry 24*, 4264−4269.
20. Wnuk, W., and Jauregui-Adell, J. (1983) *Eur. J. Biochem. 131*, 177−182.
21. Takaya, J., Higashino, H., and Kobayashi, Y. (2000) *Magn. Reson. 13*, 139−146.
22. Takagi, T., Konishi, K., and Cox, J. A. (1986) *Biochemistry 25*, 3585−3592.
23. Potter, J. D., and Gergely, J. (1975) *J. Biol. Chem. 250*, 4628−4633.
24. Potter, J. D., Robertson, S. P., and Johnson, J. D. (1981) *Fed. Proc., Fed. Am. Soc. Exp. Biol. 40*, 2653−2656.
25. Cox, J. A., and Stein, E. A. (1981) *Biochemistry 20*, 5430−5436.
26. Kohler, L., Cox, J. A., and Stein, E. A. (1978) *Mol. Cell. Biochem. 20*, 85−93.
27. Collins, J. H., Johnson, J. D., and Szent-Gyorgyi, A. G. (1983) *Biochemistry 22*, 341−345.
28. Williams, T. C., Corson, D. C., Oikawa, K., McCubbin, W. D., Kay, C. M., and Sykes, B. D. (1986) *Biochemistry 25*, 1835−1846.
29. Precheur, B., Cox, J. A., Petrova, T., Mispelter, J., and Craescu, C. T. (1996) *FEBS Lett. 395*, 89−94.
30. Creighton, T. E. (1997) *Trends Biochem. Sci. 22*, 6−10.
31. Ikura, M. (1996) *Trends Biochem. Sci. 21*, 14−17.
32. Wnuk, W., and Cox, J. A. (1982) in *Calcium and Cell Function* (Cheung, W. Y., Ed.) pp 243−278, Academic Press, New York.
33. Saris, N. E., Mervaala, E., Karppanen, H., Khawaja, J. A., and Lewenstam, A. (2000) *Clin. Chim. Acta 294*, 1−26.
34. Flatman, P. W. (1991) *Annu. Rev. Physiol. 53*, 259−271.
35. Wacker, W. E., and Parisi, A. F. (1968) *N. Engl. J. Med. 278*, 658−663.
36. Romani, A., and Scarpa, A. (1992) *Arch. Biochem. Biophys. 298*, 1−12.
37. McDonald, J. W., Silverstein, F. S., and Johnston, M. V. (1990) *Neurosci. Lett. 109*, 234−238.
38. Lucas, M. J., Leveno, K. J., and Cunningham, F. G. (1995) *N. Engl. J. Med. 333*, 201−205.
39. The Collaborative Eclampsia Trial Group (1995) *Lancet 345*, 1455−1463.
40. Goldenberg, R. L., and Rouse, D. J. (1997) *Nat. Med. 3*, 146−147.
41. Meissner, G. (1994) *Annu. Rev. Physiol. 56*, 485−508.
42. Meissner, G., and Henderson, J. S. (1987) *J. Biol. Chem. 262*, 3065−3073.
43. Arnoult, C., Kazam, I. G., Visconti, P. E., Kopf, G. S., Villaz, M., and Florman, H. M. (1999) *Proc. Natl. Acad. Sci. U.S.A. 96*, 6757−6762.
44. McCormack, J. G., Halestrap, A. P., and Denton, R. M. (1990) *Physiol. Rev. 70*, 391−425.
45. Chuang, H., Jan, Y. N., and Jan, L. Y. (1997) *Cell 89*, 1121−1132.
46. Squire, L. G., and Petersen, O. H. (1987) *Biochim. Biophys. Acta 899*, 171−175.
47. Nakayama, S., and Kretsinger, R. H. (1994) *Annu. Rev. Biophys. Biomol. Struct. 23*, 473−507.
48. Crivici, A., and Ikura, M. (1995) *Annu. Rev. Biophys. Biomol. Struct. 24*, 85−116.
49. Arai, M., and Kuwajima, K. (2000) *Adv. Protein Chem. 53*, 209−282.
50. Christova, P., Cox, J. A., and Craescu, C. T. (2000) *Proteins 40*, 177−184.
51. Findlay, W. A., and Sykes, B. D. (1993) *Biochemistry 32*, 3461−3467.
52. Sheng, Z., Strauss, W. L., Francois, J. M., and Potter, J. D. (1990) *J. Biol. Chem. 265*, 21554−21560.
53. Chen, Y. H., Yang, J. T., and Chau, K. H. (1974) *Biochemistry 13*, 3350−3359.
54. Cox, J. A., Kretsinger, R. H., and Stein, E. A. (1981) *Biochim. Biophys. Acta 670*, 441−444.
55. Cox, J. A., Winge, D. R., and Stein, E. A. (1979) *Biochimie 61*, 601−605.

BI034047J